Qiangqiang Zhang
Yang Gao
Fuwei Wang
Yaowei Yong ✉
Mengmeng Cao

https://doi.org/10.21278/TOF.494073524
ISSN 1333-1124
eISSN 1849-1391

STUDY ON THE IMPACT OF FILL GAP AND LAYER HEIGHT ON RESIDUAL STRESSES IN ARC CLADDING LAYERS IN REMANUFACTURED WIND TURBINE BROKEN GEAR TEETH

Summary

This study investigates residual stresses in arc cladding layers of wind turbine gear teeth via experiments and simulations. The results show that increasing the filling spacing from 1 mm to 3 mm reduces maximum tensile stress, decreases stress fluctuations, and mitigates heat accumulation. However, expanding the spacing to 4 mm intensifies stress fluctuations due to uneven heat input, establishing 3 mm as optimal spacing. Regarding the layer height, increasing from 2.5 mm to 3.5 mm reduces the top-layer tensile stress while creating a concave stress distribution in intermediate zones. At the 4 mm layer height, although the top-layer stress decreases, the intermediate-zone stress rises and transitions to tensile near the centre. The optimal combination – 3 mm spacing and 3.5 mm layer height – provides theoretical guidance for wire-arc additive manufacturing of failed wind turbine gears.

Key words: *wire arc additive manufacturing; fill gap; layer height; residual stress; finite element simulation*

1. Introduction

The development of wind power equipment in China is trending towards larger sizes, higher reliability, and longer service life. However, wind turbines are often located in regions rich in wind resources such as high mountains, deserts (e.g. the Gobi desert), barren beaches, and seas. In these locations, the turbines are subjected to irregular variable and variable load impacts from strong winds, as well as extreme temperature differences from severe heat to severe cold, leading to fatigue failure forms such as fractures on gear tooth surfaces after three to five years of operation, as shown in Figure 1. Typically, remanufacturing methods are employed to repair failed tooth surfaces, with common methods including adjustment and replacement, modification processing, cladding, and thermal spraying [1]. These methods have fundamental flaws: the prolonged heat-affected zones (HAZ) exceeding 2 mm depth and residual tensile stresses of 350-450 MPa in overlay welding reduce fatigue strength by 25-35%; thermal spray coatings demonstrate bonding strengths of merely 120-180 MPa, with service cycles under impact loads lasting <1.5 years [2]. These technologies remain at the surface forming stage, lacking anti-fatigue cutting capabilities and high-energy composite modification methods. They fail to resolve the three major challenges in gear design: structural weight (4 MW units weigh 14-16 tons being 20-25% heavier than international benchmarks), short lifespan (actual service life of 12-15 years vs. design life of 20 years), and poor reliability (failure rate 38-42%). Moreover, they cannot mitigate stress concentration hazards: the stress concentration coefficient at tooth fracture notches exceeds Kt=4.0-4.5, inducing localized stresses >2100 MPa. Driving cracks propagate at a rate of 1.2-6.5×10^-8 m/cycle [3], resulting in repaired gears with a lifespan less than 50% of original components. This severely hampers performance enhancement during service.

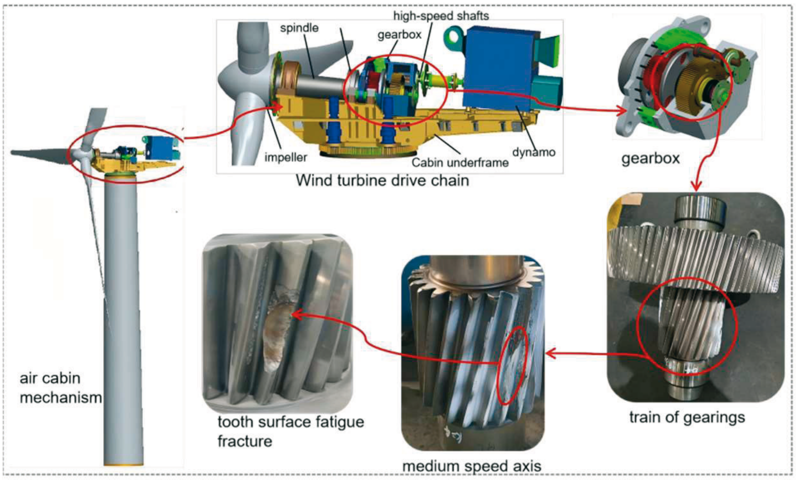

Fig. 1 Broken tooth gear in the wind turbine gearbox intermediate shaft

Driven by China's "dual carbon" goals, the wire arc additive manufacturing (WAAM) technology is gaining increasing recognition in the wind power sector and beyond. WAAM offers significant advantages in repairing failed wind turbine gears, including its capability to rapidly and accurately form complex geometries [4] and handle large-scale components [5-6]. It is particularly suitable for the remanufacturing of large and medium-sized parts such as wind turbine gears due to its high deposition efficiency [7], low working environment impact, and high material utilisation rate [8]. However, the solidification of the high-temperature molten pool can easily lead to the formation of large residual stresses in the cladding layer [9-10]. If these residual stresses surpass the material yield strength, they can induce plastic deformation. Exceeding the ultimate tensile strength can lead to the cracking of the tooth surface [11]. This significantly compromises the service life of the repaired composite surface layer [12].

In the process of metal additive manufacturing, minimising internal residual stress accumulation plays a crucial role [13]. The existing repair technologies such as thermal spraying and overlay welding exhibit significant limitations in residual stress control: thermal spraying processes generate thermal mismatch stresses and sudden cooling stresses [14], resulting in coating bonding strengths generally below 150 MPa with high susceptibility to delamination under impact loads. Overhead overlay welding creates a HAZ exceeding 2 mm depth through intense thermal input, generating residual tensile stresses of 400 MPa that reduce fatigue strength by 25-35%. Furthermore, multi-layer overlay welding induces grain boundary liquefaction cracks due to accumulated heat. These techniques rely on post-treatment (e.g. shot peening) for residual stress regulation, failing to suppress stress concentration at its source. Particularly, they cannot resolve non-uniform thermal gradients and abrupt changes in multidirectional stress during complex geometric repairs, ultimately leading to repair components with a service life less than 50% of that of the original parts [15]. Also, process parameters are among the key factors affecting the size, direction, and distribution of internal residual stresses in the arc cladding layer [9]. Ruwei Geng et al. studied the influence of different process parameters on the stress distribution in the cladding layer, finding that increasing the substrate movement speed or reducing the welding current can reduce the temperature gradient inside the molten pool, thereby mitigating residual stresses and achieving the goal of optimising residual stresses [16]. Donghong Ding et al. designed five different cladding paths and analysed the impact of different cladding paths on the internal residual stress of the cladding layer through a finite element simulation, finding extremely high residual tensile stresses near the surface of the cladding layer [17]. Wentao Han from Beijing University of Technology et al. studied the impact of different inter-layer dwell times on the distribution of internal residual stresses in single-pass multi-layer deposits, finding that the internal residual stresses were minimised when the inter-layer dwell time was between 120 and 210 s [18]. If the forced cooling technology is added to the interlayer, the internal residual stress can be minimized under the condition of reducing the cooling time [19]. Jinbiao Zhou et al. used directed energy cladding to simulate real experiments for finite element modelling, studying the impact of different scanning strategies on the internal residual stresses and temperature field of its components, and designed a reasonable scanning strategy to effectively mitigate the impact of harmful residual stresses [10]. Xuewei Fang et al. conducted research on the formation quality of single-layer multi-pass cladding layers with different overlap distances, finding that the surface flatness was optimal when the overlap distance was 0.715 times the width of a single pass [20]. Xiangman Zhou et al. studied the impact of overlap centre distance on the flow and morphology of the arc additive manufacturing molten pool. The researchers used the volume of fluid method to track the free surface of the molten pool and explored the changes in the surface temperature peak, molten pool flow, and morphology at different overlap centre distances. The results showed that changes in the overlap centre distance affected the direction and strength of the molten pool flow, thereby affecting the morphology of the deposit layer [21]. The process parameters of WAAM have a significant impact on its mechanical properties and fatigue strength [22]. Poor process parameters can directly lead to various defects in the cladding layer, affecting its mechanical properties [23].

The aforementioned studies explored the evolution patterns of temperature, residual stress, and deformation in the process of WAAM, proposing optimisation schemes for various process parameters such as welding voltage, overlap distance, and inter-layer cooling time. These provide theoretical guidance for reducing thermal accumulation, stress concentration, and internal residual stress in the cladding layer. However, most current studies focus only on the optimisation of process parameters for a small number of weld passes or unidirectional cladding. The remanufacturing of large failed components with WAAM inevitably requires cladding on known models (imported additive manufacturing slice model) to be repaired. Preliminary experiments have shown that when cladding known models, the morphology of the cladding layer and the level of internal residual stresses are greatly influenced by the process parameter of fill gap in the horizontal direction and significantly affected by the layer height in the vertical direction. Therefore, this paper aims to achieve the expected cladding effect of the predetermined model by studying the distribution pattern of internal residual stresses in single-layer multi-pass cladding layers at different fill gaps using the WAAM technology, thereby determining the optimal fill gap. Subsequently, by changing the layer height for a multi-layer multi-pass experimental design, the study investigates the impact of layer height on the residual stresses of multi-layer multi-pass cladding layers, providing theoretical support and technical guidance for a later repair of large gears. The filling spacing-layer height synergistic optimisation mechanism proposed in this study breaks through the above limitations by actively regulating the thermodynamic process. This innovation provides a low-stress forming process window for large gear remanufacturing, solves the stress concentration bottleneck of traditional repair from the source, and makes up for the technical gap in the multi-directional stress synergistic control of thermal spraying/stack welding.

2. Experimental and simulation design

2.1 Experimental design

The experimental platform for a WAAM system, as shown in Figure 2(a), was designed for single-layer multi-pass and multi-layer multi-pass cladding experiments. After extensive exploratory experiments, the final parameters were selected as shown in Table 1. The main reason is that during the single-layer multi-pass cladding experiments, the primary factor affecting the internal stress distribution is fill gap. In contrast, for multi-layer multi-pass deposition, layer height emerges as the most critical parameter influencing residual stress distribution, superseding the influence of fill gap.

Table 1 Parameters used in this study

Process parameters	Welding voltage *V*	Wire feeding speed *m/min*	Filling speed *mm/s*	Shielding gas	Scan paths
Value	20.3	5.1	14.1	80%Ar+20%CO2	Z-shaped[24]

A one-variable-at-a-time experimental approach was employed. First, in the single-layer multi-pass experiments the influence of fill gap on residual stress distribution within the deposit cross-section was analysed. Subsequently, in the multi-layer multi-pass experiments the effect of layer height on residual stress distribution in the cross-section was examined. For the single-layer experiment, a 100 mm × 24 mm × 3 mm block geometry was deposited onto a 160 mm × 120 mm × 10 mm substrate (Figure 2b). As the fill gap increased, the number of weld passes decreased. In the multi-layer multi-pass cladding experiment, a block model measuring 100 mm×24 mm×15 mm was chosen for cladding on a substrate surface measuring 160 mm×120 mm×10 mm, as shown in Figure 2(c). As the layer height increased, the number of cladding layers decreased. The welding wire material was SMSX900A with a diameter of 1.2 mm, and the base material was Q235B. The detailed composition of the raw material and base material is shown in Table 2. An X-350A stress detector was used to detect residual stresses in the cross-section of the cladding layer [25-26], with the red marked surface in Figures 2(b) and (c) chosen for residual stress testing.

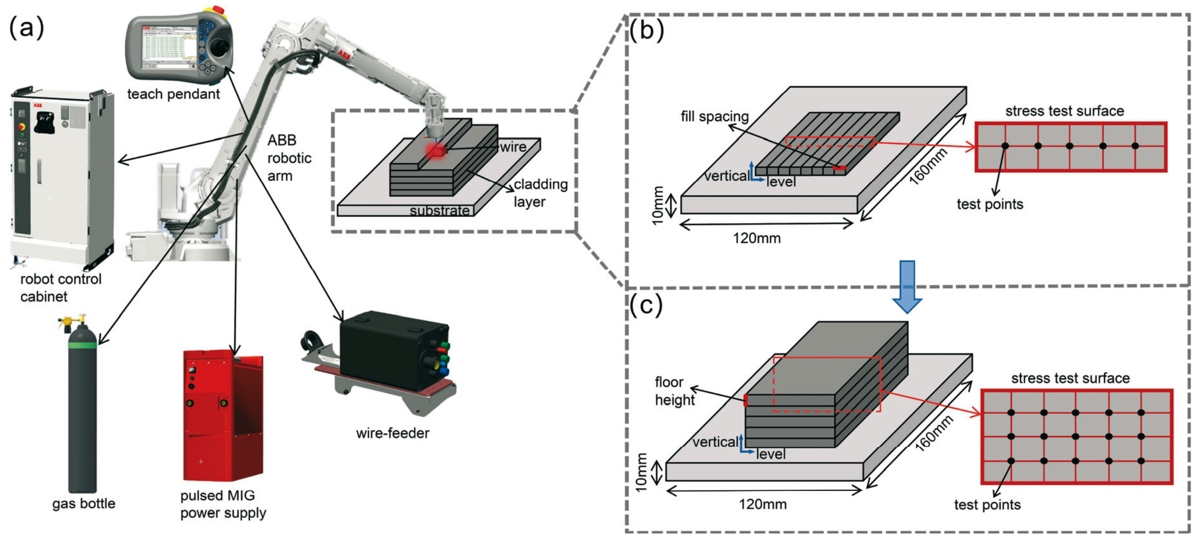

Fig. 2 Experimental platform for optimising geometric feature process parameters in wire arc additive manufacturing: (a) shows a WAAM system; (b) single-layer multi-pass schematic diagram; (c) the multi-layer multi-pass schematic diagram

Table 2 Composition of raw material (SMSX900A) and substrate (Q235B), (wt%)

Element	C	Si	Mn	Cr	Ni	Fe
SMSX900A	0.15-0.25	0.51	1.24	0.35	1.60	Bal
Q235B	0.18	0.35	0.14	N/A	N/A	Bal

In the single-layer multi-pass cladding experiment, the main process parameter affecting the residual stress distribution is the fill gap, defined as shown in Figure 2(b). In the multi-layer multi-pass cladding experiment, the main process parameter affecting the residual stress distribution is the layer height, defined as shown in Figure 2(c). Therefore, this study investigated: (1) the influence of varying fill gaps on internal residual stress distribution in single-layer multi-pass deposits; and (2) the effect of layer height on internal residual stresses within multi-layer multi-pass deposits. Preliminary experiments established a feasible range of process parameters (excluding filler gap and layer height) for forming a sound cladding layer. These trials revealed that a zigzag scanning path yielded superior results compared to linear and square paths. This finding aligns with conclusions reported in the literature [17]. Therefore, the zigzag scanning path was chosen, with specific parameters shown in Table 1. Based on preliminary experiments, the following parameter ranges and increments were defined for testing: 1) Fill gap: 2.5–4 mm (in 0.5 mm increments) for single-layer multi-pass experiments (Table 3); Layer height: 1–4 mm (in 1 mm increments) for multi-layer multi-pass experiments (Table 4).

Table 3 Single-layer and multichannel process parameters

Test number	1	2	3	4
Fill spacing (*mm*)	1	2	3	4

Table 4 Multi-layer and multichannel process parameters

Test number	1	2	3	4
Floor height (*mm*)	2.5	3	3.5	4

2.2 Finite element modelling and simulation using Simufact

Using the process parameters established in the preliminary experiments (Table 1), the Simufact Welding software simulated both single-layer multi-pass and multi-layer multi-pass WAAM deposition processes. The simulation incorporated the following key assumptions relevant to the process characteristics: 1) constant heat source input power (time-invariant); 2) simplified heat conduction between heat source and workpiece via thermal efficiency η [27]; 3) explicit modelling of convective heat transfer and thermal radiation between the deposit/substrate and deposit/air interfaces within a finite element model [28-29]. The simulation process mainly involves two steps: 1) the three-dimensional modelling and mesh division of the substrate and cladding layer, along with the parameter setting for the double-ellipsoidal heat source; 2) the planning of the welding gun cladding path using cell generation technology. The equivalent stress field of the cladding layer was obtained by simulating different experiments through changing boundary conditions.

Currently, typical heat source models include the Rosenthal heat source model [30], the Gaussian heat source model [31], and a double-ellipsoidal heat source model. While computationally simpler, the Gaussian model fails to account for arc stiffness effects on the molten pool in deep-penetration welding processes. This limitation is particularly pronounced in multi-layer multi-pass welds. Consequently, the Gaussian model cannot accurately represent the arc penetration power, resulting in significant deviations between the simulated and the measured results. The double-ellipsoidal model, researched by Goldak et al. [32] while studying the power density distribution of welding arcs, reflects the heat distribution in a molten pool well. The geometric model of the heat source is shown in Figure 3, and the power density function is as shown by Equation (1):

$$q=\frac{6\sqrt{3}f_{1,2}Q}{\pi^{3/2}a_{f,r}bc}\exp\left[-3\left(\frac{x^2}{a_{f,r}^2}+\frac{y^2}{b^2}+\frac{z^2}{c^2}\right)\right] \quad z<0 \tag{1}$$

where q represents the heat source power density; $f_{1,2}$ are the heat distribution coefficients of the front and rear hemispheres, respectively, with f_1=0.6, f_2=1.4; a_r, a_f, b, and c are the geometric parameters of the heat source model, chosen based on the actual size of the molten pool as shown in Table 5; Q is the power transferred to the molten pool, $Q=\eta IU$, where η, I and U represent the welding thermal efficiency, current and voltage, respectively. This model consists of two 1/4 ellipsoids, front and rear, with four shape parameters: a_f, a_r, b, and c. The energy distribution coefficients of the front and rear ellipsoids are f_1 and f_2. So, to accurately calculate the stress field, the four parameters of the heat source need to be verified, where a_f is the length of the first half ellipsoid, a_r is the length of the second half ellipsoid, b is the width of the half ellipsoid, and d is the depth of the ellipsoid.

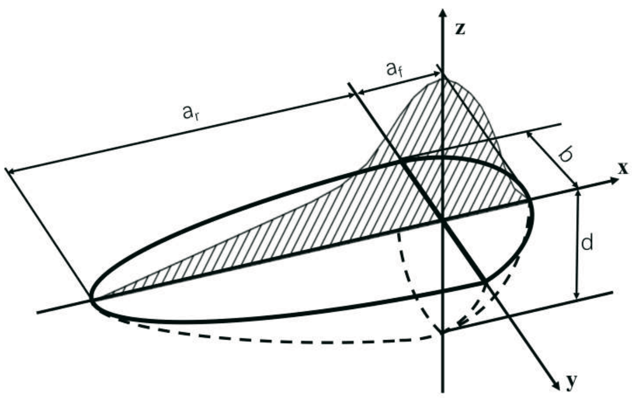

Fig. 3 Schematic diagram of the double ellipsoidal heat source model

Table 5 Heat source model parameters

Parameter	a_r /mm	a_f /mm	b /mm	d /mm	η
Value	9	2.9	3.5	4.1	0.7

Consistent with the experiment, the substrate size in both the single-layer single-pass and multi-layer multi-pass simulation models was chosen to be 160 mm×120 mm×10 mm. The substrate was divided into a hexahedral mesh measuring 5×5×5, as shown in Figure 4. For the single-layer multi-pass simulation, the overall size of the cladding layer was 100 mm×24 mm×3 mm. By changing the size and number of weld passes, the simulation aimed to achieve the effect of changing the fill gap, as shown in Figure 4(a). For the multi-layer multi-pass simulation, the overall size of the cladding layer was 100 mm×24 mm×15 mm. By changing the thickness of a single cladding layer and the number of layers, the simulation aimed to achieve the effect of changing the layer height, as shown in Figure 4(b). During modelling and simulation, the geometric model was created and unnecessary chamfers and geometric features were cleaned up.

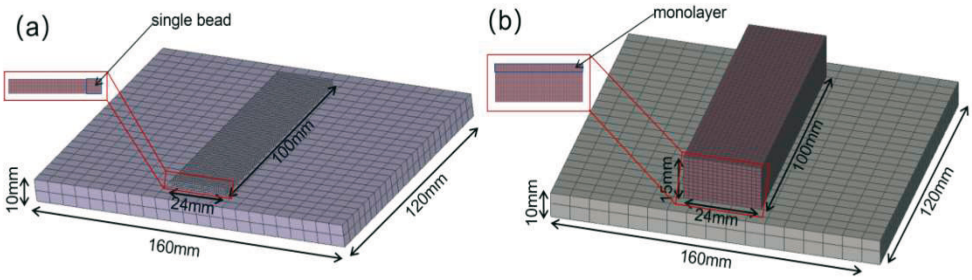

Figure 4 Model establishment and mesh division: (a) single-layer multi-pass model diagram; (b) multi-layer multi-pass model diagram

3. Results and discussion

3.1 The impact of fill gap on the internal residual stress in single-layer multi-pass cladding layers

The internal residual stress within the cladding layer is primarily caused by its non-uniform temperature gradient. The fill gap significantly influences the internal temperature distribution of the cladding layer. Figure 5 presents temperature contour maps captured at the moment of arc extinguishing for gaps of 1 mm, 2 mm, 3 mm, and 4 mm. Figure 5 reveals that as the filler gap increases, the extent of the high-temperature region gradually diminishes. This reduction is particularly pronounced in the thermal diffusion zone of the substrate. With the continuous increase of the fill gap, the high-temperature range on the substrate gradually decreases. Therefore, in single-layer multi-pass cladding, a decreasing filler gap, resulting from adding more passes within a fixed width, leads to denser pass spacing. This denser spacing prolongs heat accumulation in the horizontal direction.

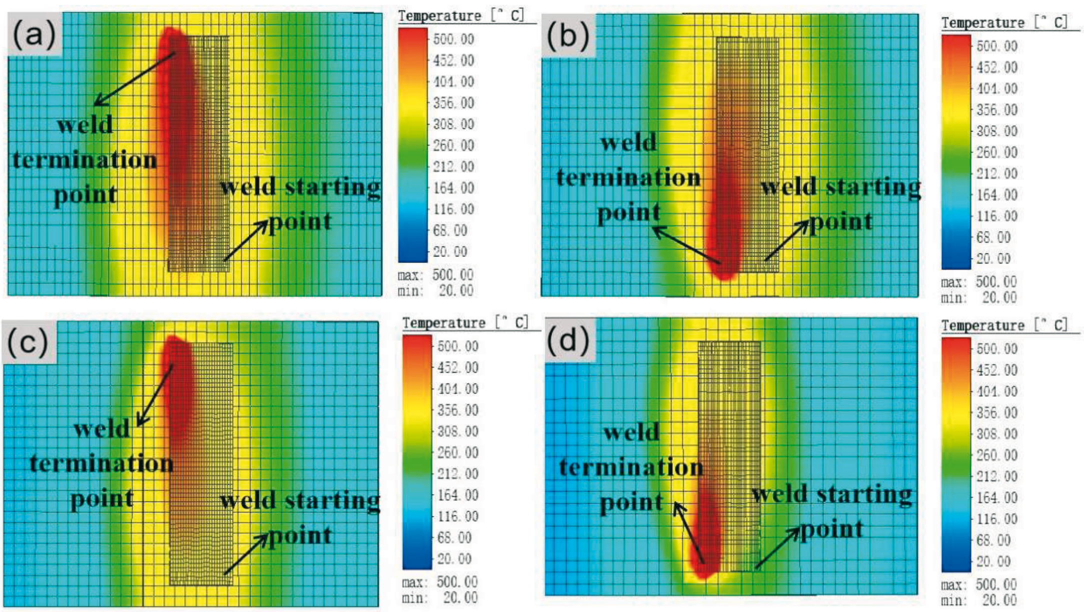

Fig. 5 Temperature contour maps of single-layer multi-pass cladding layers at different fill gaps: (a) fill gap of 1 mm; (b) fill gap of 2 mm; (c) fill gap of 3 mm; (d) fill gap of 4 mm

Consequently, the substrate receives more heat input, expanding the high-temperature region near the weld pass and enlarging the HAZ. Furthermore, the increased cooling time per pass confines the high-temperature zone more closely to the molten pool region. Conversely, an increasing filler gap shortens the overall heat accumulation time. Under this condition, individual passes lack sufficient time to dissipate heat, leading to an expansion of their high-temperature regions. Simultaneously, the surrounding substrate receives insufficient heat input to significantly expand the HAZ. However, an excessively large filler gap results in overly sparse pass spacing, compromising the formation quality of the cladding layer.

By changing the size of a single-weld pass model, a finite element simulation was conducted on single-layer multi-pass cladding layers at different fill gaps. The simulation results reveal that residual stresses within the cladding layer are predominantly tensile. Significant stress concentration occurs at the cladding path endpoint, resulting in elevated residual stresses at this location. When the fill gap is 1 mm, the area of the red high-temperature region at the extinguishing end is the largest, and the residual tensile stress value is the highest. As the fill gap increases, the area of the red high-temperature region at the extinguishing end gradually decreases. When the fill gap increases to 3 mm, as shown in Figure 6(c), the stress distribution of the cladding layer is relatively uniform. When the fill gap further increases to 4 mm, due to the too few number of weld passes, as shown in Figure 6(d), the stress distribution of the cladding layer shows an uneven distribution.

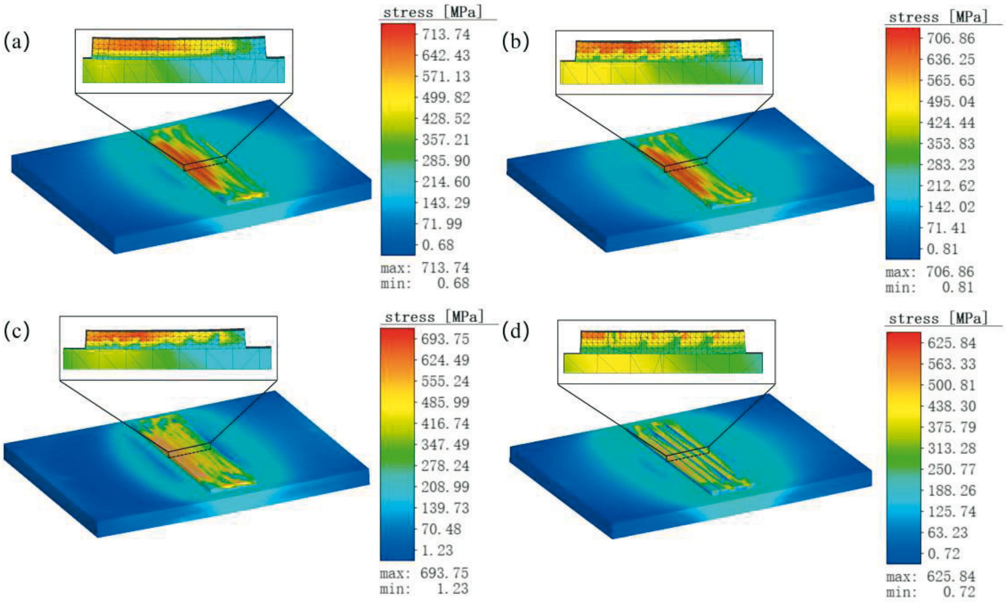

Fig. 6 Stress contour maps of cladding layers cooled to room temperature at different fill gaps: (a) fill gap of 1 mm; (b) fill gap of 2 mm; (c) fill gap of 3 mm; (d) fill gap of 4 mm

Figure 7 shows the internal residual stress distribution in the horizontal direction of the arc cladding layer, with Exp denoting experimental values and Sim denoting simulation values. Figure 8 shows the change in weld height of single-layer multi-pass cladding layers at different fill gaps, with the testing position consistent with the residual stress testing position. The maximum residual stress value for all cladding layers is 501 MPa, below the yield strength of the material (832 MPa). When the fill gap is 1 mm (i.e., Exp-1 mm, Sim-1 mm), the small fill gap causes an excessive overlap rate of weld passes, continuously adding to the thickness of the cladding layer, with continuous input of arc heat, making the thermal accumulation effect obvious [33], as shown in Figure 7. From the geometric morphology of the cladding layer, the weld height along the horizontal cladding direction shows an increasing trend, with overly dense weld passes, the weld height of the cladding layer increases along the horizontal cladding path, and due to the temperature rise from the previous welding, the thermal accumulation continues to add up, ultimately leading to stress concentration. Therefore, the internal residual stress in the horizontal direction increases overall, in line with the trend of the weld bead geometry. At the extinguishing end, the weld height is relatively large; heat accumulates and dissipates slowly. Consequently, thermal expansion and contraction produce higher residual stress [33], and stress concentrates on this side, leading to poor bead appearance, as shown in Experiment 4 presented in Figure 8.

Increasing the fill gap to 3 mm reduces the number of deposition layers and overlap. This mitigates the heat accumulation and promotes a more uniform heat distribution. Consequently, the stress concentration weakens, the residual stress fluctuations smooth out significantly in the horizontal direction, and the cladding layer height distribution becomes uniform (Figure 8). The reduced local heat buildup and the more even arc heat distribution lead to minimised stress fluctuations. At a fill gap of 4 mm (Exp-4 mm, Sim-4 mm), the significant decrease in overlap leads to an uneven weld height distribution, manifesting as a convex profile (higher centre, lower edges). Furthermore, the cladding layer thickness diminishes towards the centre. This geometric non-uniformity exacerbates the uneven heat distribution. As a result, the residual stress distribution becomes more dispersed throughout the cladding layer (Figure 8). Notably, the simulated stress distribution pattern corresponds closely to the geometric morphology and aligns well with the experimental measurements. The results indicate that the cladding effect is optimal when the fill gap is 3 mm.

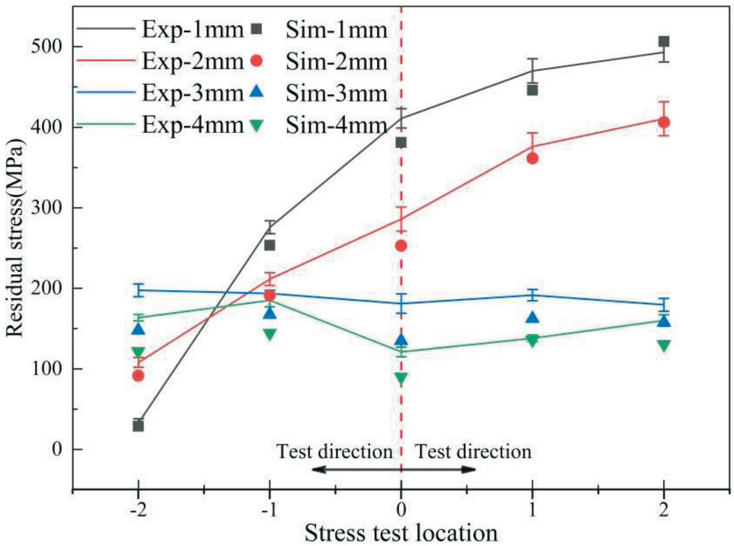

Fig. 7 Stress distribution at different fill gaps

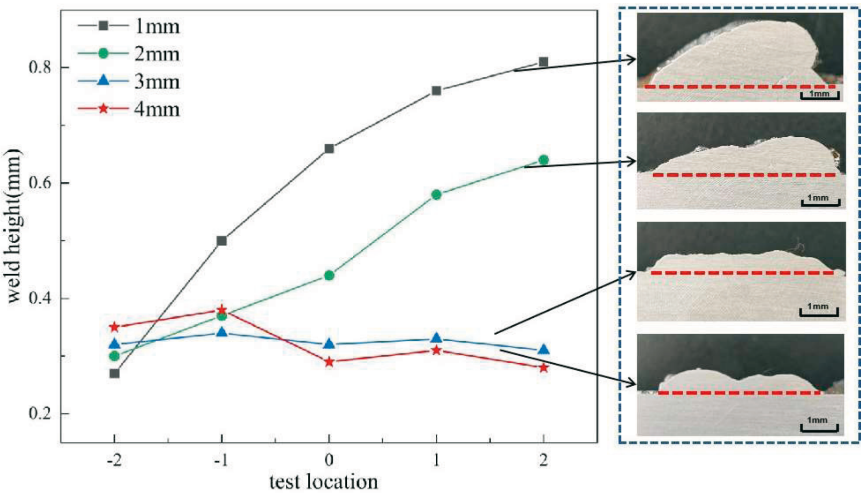

Fig. 8 Distribution of weld height in the cross-section of single-layer multi-pass cladding layers at different fill gaps

3.2 The impact of layer height on the internal residual stress in multi-layer multi-track cladding layers

For the multi-layer multi-track cladding experiments, the key process parameters welding voltage, wire feeding speed, and travel speed were fixed. Among the remaining variables, layer height emerged as the primary factor governing the internal residual stress distribution within the cladding layer. This is because the layer height directly influences the temperature distribution during deposition. Therefore, to study the impact of different layer heights on the internal residual stress distribution of multi-layer multi-track cladding layers, the impact on the temperature distribution of the cladding layer was first investigated. Figure 9 displays the temperature cloud diagrams of multi-layer multi-track cladding layers with different layer heights. It can be seen from the figure that as the layer height decreases, the high-temperature region becomes larger, and the molten pool temperature is higher. When the layer height is 4 mm, the highest temperature of the molten pool is 1,919.43 °C, with a very small high-temperature region. As the layer height continuously decreases, the number of cladding layers continuously increases, the high-temperature region gradually becomes larger, and the molten pool temperature gradually increases. Critically, the initiation of each new layer occurs over a still-hot region from the previous layer that has not sufficiently cooled. This pre-heated zone, lacking adequate time for heat dissipation, receives additional heat input, leading to a significant heat buildup. When the layer height is 2.5 mm, the thermal accumulation phenomenon is the most severe, and the high-temperature region is the largest, with the highest temperature of the molten pool reaching 4,032.21 °C.

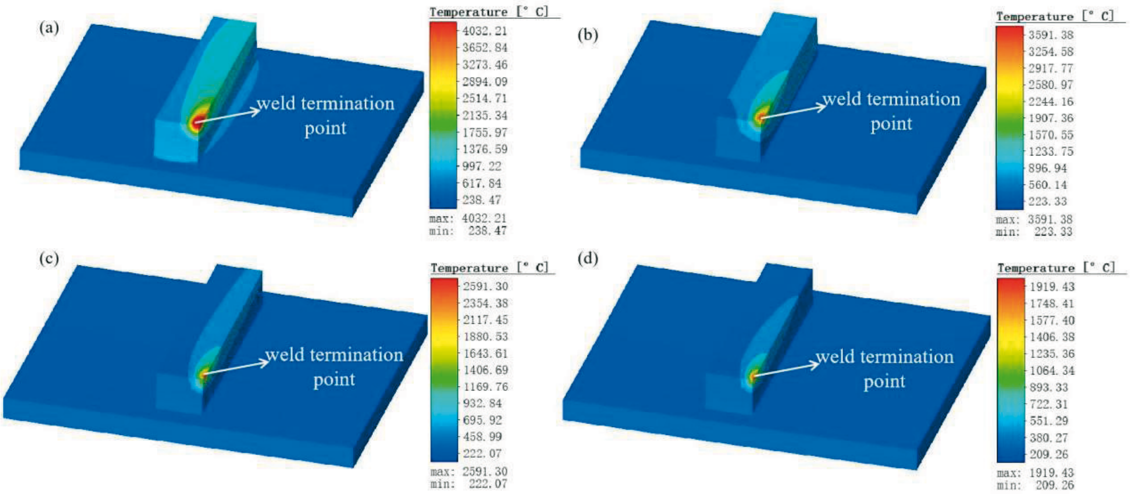

Fig. 9 Temperature cloud diagrams of multi-layer multi-track cladding layers with different layer heights: (a) layer height of 2.5 mm; (b) layer height of 3 mm; (c) layer height of 3.5 mm; (d) layer height of 4 mm

Figure 10 shows the Y-direction stress distribution cloud diagrams of multi-layer multi-track cladding layers with different layer heights. A finite element simulation was conducted on cladding layers with different layer heights, and the Y-direction normal stress components of cladding layers with layer heights of 2.5 mm, 3 mm, 3.5 mm, and 4 mm were analysed. The analysis of Figure 10 reveals two key features: 1) The top surface layer exhibits substantial residual tensile stress; 2) Significant stress variation occurs near the arc extinguishing end due to the abrupt termination of heat input. Specifically, the residual tensile stresses within the weld track at this end markedly exceed levels observed elsewhere in the cladding layer. Within the middle region of the cladding layer, stress levels decrease significantly, approaching zero. Furthermore, a portion of the residual tensile stresses transitions into compressive residual stresses. Notably, the highest stresses within this middle layer occur near the cladding ends.

This localisation arises because direct exposure to ambient air creates steep temperature gradients during cooling, resulting in elevated residual stresses at the ends compared to the central middle zone. At the minimum layer height of 2.5 mm, the top layer exhibits the peak residual tensile stress value. Conversely, the middle layer displays its maximum extent of compressive residual stress area. Progressively increasing the layer height reduces the number of deposition layers. This trend correlates with a decrease in the residual tensile stresses at the top layer. However, within the middle layer, the compressive residual stress zone shrinks, and correspondingly, a substantial area transitions, exhibiting tensile residual stresses.

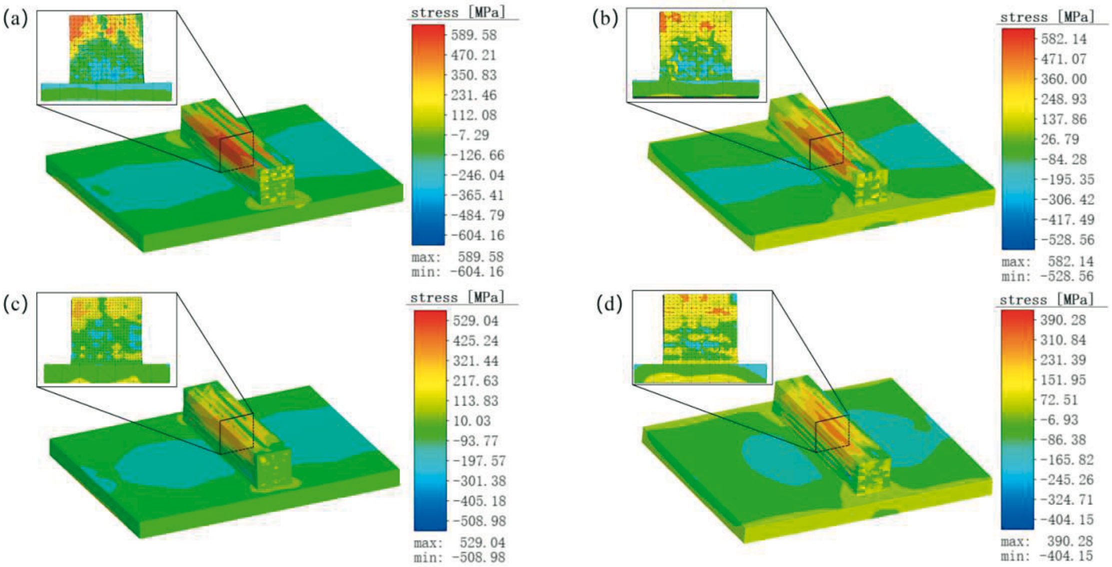

Fig. 10 Stress cloud diagrams of multi-layer multi-track cladding layers with different layer heights: (a) layer height of 2.5 mm; (b) layer height of 3 mm; (c) layer height of 3.5 mm; (d) layer height of 4 mm

The internal residual stress distribution of multi-layer multi-track cladding layers with different layer heights was extracted, with the location of a selected testing point as shown in Figure 2(c). Figure 11 shows the impact distribution diagram of layer height on the stress of multi-layer multi-track cladding layers (Exp for experimental values, Sim for simulation values): Figure 11(a) displays a stress distribution diagram for a layer height of 2.5 mm; Figure 11(b) for a layer height of 3 mm ; Figure 11(c) for a layer height of 3.5 mm; Figure 11(d) for a layer height of 4 mm. It can be observed that the sectional stress of the cladding layer gradually increases from the bottom of the substrate to the top of the component, with the middle region showing residual compressive stresses, and the region near the top of the cladding layer shows residual tensile stresses. The melting and solidification of a metal wire is a process of thermal expansion and cooling contraction, with the region near the top of the cladding layer directly contacting the air medium during the cooling and solidification process, experiencing a large temperature change gradient, and being restricted by surrounding conditions, thus presenting as residual tensile stress [33], which is consistent with the simulation results given in [17]. When the layer height is 2.5 mm, the maximum residual tensile stress value at the top layer of the cladding layer is 525 MPa. Increasing the layer height beyond 2.5 mm results in a concave residual stress profile near the substrate in the horizontal direction. Concurrently, the stress gradient diminishes, and the magnitude of the residual tensile stresses decreases. This occurs because, for a given cladding volume model, a higher layer height reduces the number of required cladding layers. Consequently, the cumulative arc heat input decreases, resulting in a lower stress gradient. The closer to the substrate, the smaller its residual stress, with most stresses being residual compressive stresses, except for some residual tensile stresses. The closer to the substrate, the larger the value of the compressive stress, because the subsequent cladding layers effectively act as a heat treatment to the previous layer, with each layer remelting the previous layer to some extent, thereby reducing its stress concentration phenomenon [34]. As the layer height increases, the residual tensile stress value at the top layer of the cladding layer decreases. When the layer height is 3 mm, the maximum tensile stress is 481 MPa, a decrease of 44 MPa compared to a layer height of 2.5 mm. The stress values at both ends of the middle region of the cladding layer also decrease, because as the layer height continuously increases, the number of cladding layers continuously decreases, and the thermal accumulation phenomenon of the cladding layer decreases. When the layer height increases to 3.5 mm, the maximum residual tensile stress value at the top layer is 328 MPa, with the smallest thermal accumulation phenomenon in this area, and the smallest horizontal fluctuation in the residual stress distribution. The stress value in the middle region of the cladding layer has minimal horizontal fluctuation, close to zero. When the layer height continues to increase to 4 mm, the number of cladding layers is too few, not only causing the weld height of the cladding layer to be too small, differing greatly from the cladding model, but also leading to an uneven distribution of residual stress at the top layer of the cladding layer, with the horizontal distribution presenting a convex distribution, and the maximum residual tensile stress near the centre of the cladding layer, consistent with the simulation results. Due to severe thermal accumulation near the middle of the cladding, the heat from the previous cladding layer has not fully dissipated, and the subsequent cladding layer continues to receive heat, leading to stress concentration, while the stress values closer to both ends decrease, because the cladding layer ends are directly in contact with the air, with less thermal accumulation compared to the cladding centre, and still subjected to the remelting effect of the previous cladding layer, thus the top layer of the cladding layer presents a convex distribution of residual tensile stresses. Due to the thermal accumulation effect being greater than the remelting effect, the middle region of the cladding layer causes the stress value to be the residual tensile stress.

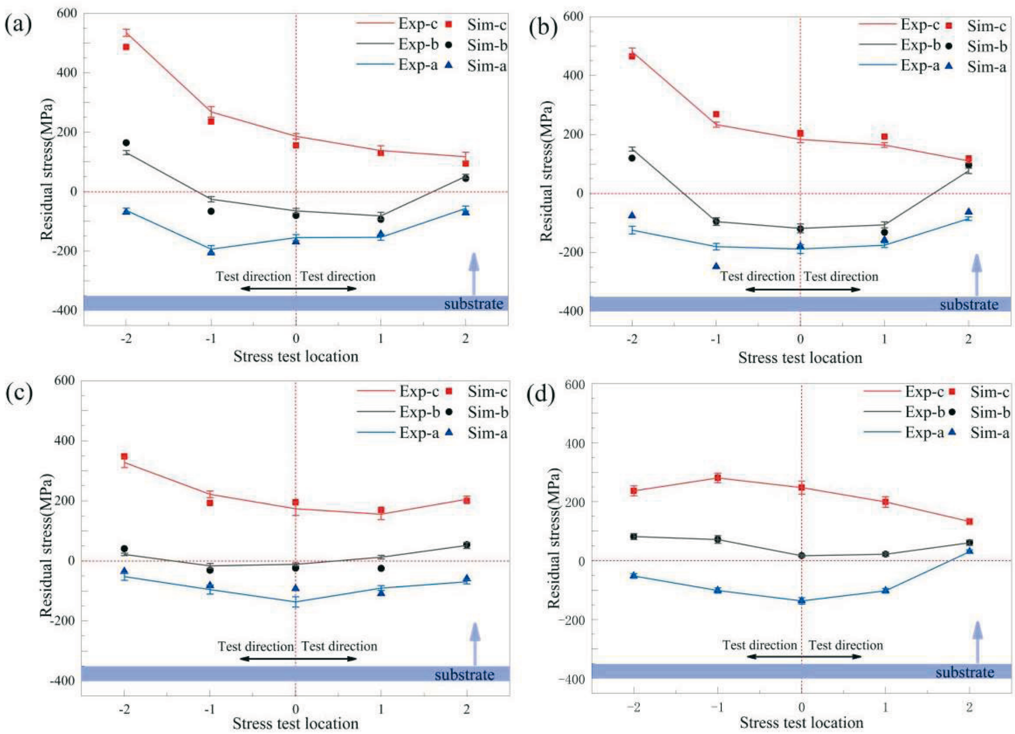

Fig. 11 Influence of layer height on stress distribution of multi-channel cladding layers: (a) layer height of 2.5 mm; (b) layer height of 3 mm; (c) layer height of 3.5 mm; (d) layer height of 4 mm

Figure 12 presents cross-sectional measurements of the weld height and width in the multi-layer multi-track cladding. The results show that the weld width remains almost constant. This stability arises because the number of horizontal weld tracks is fixed for a given cladding model. In contrast, the weld height exhibits a more pronounced variation. As the layer height increases, its weld height gradually decreases. The height of the cladding model is 15 mm, and when the layer height is 3.5 mm, its weld height is 15.2 mm, which is the closest to the model size. Therefore, considering both the residual stress distribution across the cladding cross-section and its geometric morphology (primarily the weld height conformity), the optimal cladding quality is achieved at a layer height of 3.5 mm.

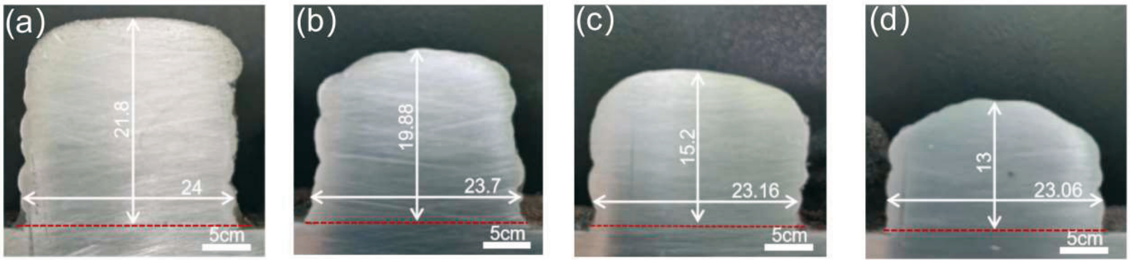

Fig. 12 Section morphology of different layers: (a) layer height of 2.5 mm; (b) layer height of 3 mm; (c) layer height of 3.5 mm; (d) layer height of 4 mm

4. Conclusions

This study employed a combined experimental and simulation approach. Single-layer multi-track and multi-layer multi-track experiments, along with a finite element analysis, were designed to investigate: 1) the influence of filler gap on the internal residual stress distribution within single-layer multi-track cladding; 2) the impact of layer height on the internal residual stress distribution within multi-layer multi-track cladding. The key findings are as follows:

1. Based on a double ellipsoid heat source model, we established a thermodynamic model. This model effectively assesses variations in the internal stress distribution within the cladding layer under different process parameters. This method can be applied to calculate the WAAM process of workpieces with complex geometric shapes.
2. The filling gap has a significant impact on the temperature field and internal residual stress distribution of a single-layer multi-track cladding layer. For the same cladding model, a smaller filling gap results in a larger number of weld tracks in a single-layer multi-track cladding layer, leading to more severe thermal accumulation and consequently stress concentration phenomena. Conversely, too small a filling gap causes an uneven heat distribution and an uneven internal residual stress distribution. The analysis of the experimental and finite element simulation results indicates that a filling gap of 3 mm is optimal.
3. Layer height significantly affects the temperature field and internal residual stress distribution of multi-layer multi-track cladding layers. For a given multi-layer cladding geometry, a smaller layer height necessitates more layers to achieve the required build height. This configuration leads to elevated residual tensile stresses in the top region. Conversely, the middle region predominantly exhibits residual compressive stresses. This stress state shift arises because the remelting effect from subsequent weld passes reduces the temperature gradient, diminishing the thermal contraction stresses in the middle zone. Conversely, an excessively high layer height results in fewer cladding layers. Under this condition, the remelting effect from

subsequent passes is diminished, and heat accumulation becomes more pronounced. Consequently, the middle region of the cladding layer develops residual tensile stresses. The analysis of the experimental and finite element simulation results shows that a layer height of 3.5 mm is optimal.

4. By integrating the experimental and the simulation results, it was found that a filling gap of 3 mm and a layer height of 3.5 mm yield the most ideal internal residual stress distribution in multi-layer multi-track cladding layers. This provides valuable guidance for the repair of wind turbine gear failures by using WAAM.

Acknowledgments

This research was funded by the Ningxia Natural Science Foundation, grant number 2024AAC03057, the Ningxia Natural Science Foundation, grant number 2023AAC02047, the Ningxia Leading Talents in Science and Technology Program, grant number 2024GKLRLX03, the Science Foundation of North Minzu University, grant number 2023QNPY13, the Science Foundation of North Minzu University, grant number 2024XYZJD01, the Ningxia Engineering Research Center for Hybrid Manufacturing System Foundation, grant number 2023GCJS008 and the Ningxia University Innovation Project, grant number CXXM2025101.

REFERENCES

[1] Zhao L., & Shi H. (2007). Overview on gear transmission wear and its repair. Proceedings of the CSC, 5(002), 243-247.

[2] Zhou, X., Jiang, W., Liu, H., Yang G. (2014). Bending stress and crack characteristics at the tooth root of a wind power gear Modern Machinery, (6), 24-28.

[3] Zhang, X., Zhong, J., Li, W. (2024). Crack Fault Characteristic Analysis of a Wind Turbine Gearbox with Flash Temperature Considered. Mechanical Science and Technology for Aerospace Engineering, 43(2), 187-196.

[4] Costello, S. C., Cunningham, C. R., Xu, F., Shokrani, A., Dhokia, V., & Newman, S. T. (2023). The state-of-the-art of wire arc directed energy deposition (WA-DED) as an additive manufacturing process for large metallic component manufacture. International Journal of Computer Integrated Manufacturing, 36(3), 469-510. https://doi.org/10.1080/0951192X.2022.2162597

[5] Wang, C., Wang, J., Bento, J., Ding, J., Pardal, G., Chen, G., & Williams, S. (2023). A novel cold wire gas metal arc (CW-GMA) process for high productivity additive manufacturing. Additive Manufacturing, 73, 103681. https://doi.org/10.1016/j.addma.2023.103681

[6] Kumar, N., Bhavsar, H., Mahesh, P. V. S., Srivastava, A. K., Bora, B. J., Saxena, A., & Dixit, A. R. (2022). Wire arc additive manufacturing-a revolutionary method in additive manufacturing. Materials chemistry and physics, 285, 126144. https://doi.org/10.1016/j.matchemphys.2022.126144

[7] Zhang Y., Wu B., Zhao Y., Ding D., Pan Z., & Li H. (2024). Research Progress in the Numerical Simulation of Heat and Mass Transfer during Wire Arc Additive Manufacturing. Journal of Mechanical Engineering, 60(8), 65-80.

[8] Yu Q., Cheng Y., Wei Y., Chen J., Hao Z., & Ao S. (2023). Review on shape control and online monitoring of wire and arc additive manufacturing (WAAM). Welding Technology, 52(3), 1-13.

[9] Bai C. (2021). Study on the Evolution of Residual Stress in Multi-layer and Multi-pass Laser Cladding (Doctoral dissertation). China University of Mining and Technology.

[10] Zhou, J., Barrett, R. A., & Leen, S. B. (2022). Three-dimensional finite element modelling for additive manufacturing of Ti-6Al-4V components: Effect of scanning strategies on temperature history and residual stress. Journal of Advanced Joining Processes, 5, 100106. https://doi.org/10.1016/j.jajp.2022.100106

[11] Song, X., Feih, S., Zhai, W., Sun, C. N., Li, F., Maiti, R., & Korsunsky, A. M. (2020). Advances in additive manufacturing process simulation: Residual stresses and distortion predictions in complex metallic components. Materials & design, 193, 108779. https://doi.org/10.1016/j.matdes.2020.108779

[12] Shamsaei, N., & Simsiriwong, J. (2017). Fatigue behaviour of additively-manufactured metallic parts. Procedia Structural Integrity, 7, 3-10. https://doi.org/10.1016/j.prostr.2017.11.053

[13] Vastola, G., Zhang, G., Pei, Q. X., & Zhang, Y. W. (2016). Controlling of residual stress in additive manufacturing of Ti6Al4V by finite element modeling. Additive Manufacturing, 12, 231-239. https://doi.org/10.1016/j.addma.2016.05.010

[14] Zhao, J. (2009). Study on the formation of residual stress in thermal spray coatings and its control factors. Shenyang University of Technology.

[15] Luo, R. (2008). Research and analysis of stress in thermal spray coatings. Wuhan University of Technology.

[16] Geng R., Cheng Y., Du J., & Wei Z. (2023). Research on Temperature Field and Stress Evolution of 2319 Aluminum Alloy in Wire and Arc Additive Manufacturing. Materials Reports, 37(23), 165-172.

[17] Ding, D., Huang, R., Liu, T., Yuan, L., & Liu, C. (2024). Effects of path patterns on residual stresses and deformations of directed energy deposition-arc built blocks. Virtual and Physical Prototyping, 19(1), e2296128. https://doi.org/10.1080/17452759.2023.2296128

[18] Han W., Lin J., Lei Y. & Ge J. (2019). Thermodynamic behavior of 2Cr13 thin-walled parts for arc additive manufacturing under different interlayer residence times. Transactions of the China Welding Institution,40(12),7.

[19] Zhang Y., Shao D., Ding D., & Wu B. (2023). Effect of Active Interpass Cooling on Temperature and Thermal Stress Evolution of Wire Arc Additively Manufactured Ti6Al4V Alloy. Electric Welding Machine, 53(2), 111-116.

[20] Fang X., Bai H., Yao Y., Zhang L., & Lu B. (2020). Research on Multi-bead Overlapping Process of Wire and Arc Additive Manufacturing Based on Cold Metal Transfer. Journal of Mechanical Engineering, 56(1), 7. https://doi.org/10.3901/JME.2020.01.141

[21] Zhou X., Wang Y., Wang L., Bai X., Fu J., & Tian Q. (2024). Numerical simulation of effect of overlapping distance on molten pool flow and deposited layer morphology of WAAM. Journal of Materials and Heat Treatment, 45(3), 195-204.

[22] Sanaei, N., & Fatemi, A. (2021). Defects in additive manufactured metals and their effect on fatigue performance: A state-of-the-art review. Progress in Materials Science, 117, 100724. https://doi.org/10.1016/j.pmatsci.2020.100724

[23] Xu, X., Ding, J., Ganguly, S., & Williams, S. (2019). Investigation of process factors affecting mechanical properties of INCONEL 718 superalloy in wire+ arc additive manufacture process. Journal of Materials Processing Technology, 265, 201-209. https://doi.org/10.1016/j.jmatprotec.2018.10.023

[24] Feng, Y. (2024). Research on remanufacturing process of fatigue fracture gear with material addition/reduction. North Minzu University.

[25] Zhang, Y., Kong, D., Yin, S. M., Feng, A., Lu, J., & Ge, T. (2006). Study on residual stress of AISI304 TIG welding line with laser shock processing by X-ray stress analyzer. In Proceedings of the Second International Symposium on Advanced Optical Manufacturing and Testing Technologies: Optical Test and Measurement Technology and Equipment, 6150, 322-326). https://doi.org/10.1117/12.676412

[26] Tian, J., Xu, P., Chen, J., & Liu, Q. (2019). Microstructure and phase transformation behaviour of a Fe/Mn/Si/Cr/Ni alloy coating by laser cladding. Optics and Lasers in Engineering, 122, 97-104. https://doi.org/10.1016/j.optlaseng.2019.06.003

[27] Zhang Q. (2018). Determination of the Parameters of Double Ellipsoid Heat Source Model and Its Application in Simulation of Multi-pass Welding (Doctoral dissertation). China University of Petroleum (East China).

[28] Deng D., Tong Y., & Zhou Z. (2011). Numerical modeling of welding distortion in thin-walled mild steel pipe. Transactions of the China Welding Institution, 32(2), 4.

[29] Deng D., & Kiyoshima S. (2011). Influence of welding sequence on welding residual stress distribution in thick plate joint. Transactions of the China Welding Institution, 32(12), 4.

[30] Rosenthal, D. (1941). Mathematical theory of heat distribution during welding and cutting. Welding journal, 20(5), 220s-234s.

[31] Pavelic, V. (1969). Experimental and computed temperature histories in gas tungsten arc welding of thin plates. Welding Journal Research Supplement, 48, 296-305.

[32] Goldak, J., Chakravarti, A., & Bibby, M. (1984). A new finite element model for welding heat sources. Metallurgical transactions B, 15, 299-305. https://doi.org/10.1007/BF02667333

[33] Wu C., Lei W., Li X., & Cong M. (2024). Thermodynamic Analysis of Single-layer Multi-pass Wire Arc Additive Manufacturing under Different Paths. Hot Working Technology, 53(7), 16-22.

[34] Zhou X., Qin J., Tian Q., Du Y., & Fu J. (2021). Effect of double-sided deposition on deformation and stress of wire arc additive manufacturing wall parts. Welding & Joining (12), 8.

Submitted: 26.11.2024

Accepted: 03.8.2025

Qiangqiang Zhang
School of Mechanical Engineering, Ningxia University, Yinchuan 750021, China

Yang Gao
Fuwei Wang
College of Mechatronic Engineering, North Minzu University, Yinchuan 750021, China

Yaowei Yong*
Mengmeng Cao
School of Mechanical Engineering, Ningxia University, Yinchuan 750021, China

*Corresponding author: yywnxu@163.com